

Svortices and the fundamental modes of the “snake instability”: Possibility of observation in the gaseous Bose–Einstein Condensate

Joachim Brand and William P. Reinhardt

Department of Chemistry, University of Washington, Seattle, WA 98195-1700, USA

(November 20, 2018)

The connection between quantized vortices and dark solitons in a long and thin, waveguide-like trap geometry is explored in the framework of the non-linear Schrödinger equation. Variation of the transverse confinement leads from the quasi-1D regime where solitons are stable to 2D (or 3D) confinement where soliton stripes are subject to a transverse modulational instability known as the “snake instability”. We present numerical evidence of a regime of intermediate confinement where solitons decay into single, deformed vortices with solitonic properties, also called svortices, rather than vortex pairs as associated with the “snake” metaphor. Further relaxing the transverse confinement leads to production of 2 and then 3 vortices, which correlates perfectly with a Bogoliubov–de Gennes stability analysis. The decay of a stationary dark soliton (or, planar node) into a single svortex is predicted to be experimentally observable in a 3D harmonically confined dilute gas Bose–Einstein condensate.

03.75.-b, 05.45.Yv, 42.65.Tg

Solitons and quantized vortices are fundamental excitations of non-linear media. Quantized vortices, often regarded as an indicator for superfluidity, are topological defects in (2+1)- or (3+1)-dimensional fluids. Dark solitons, in their purest form are solitary, nondispersive density-notch solutions to (1+1)-dimensional, non-linear wave equations with extraordinary stability properties. It has been known, however, for many years that solitonic wave fronts (also called band solitons or soliton stripes) in 2- or 3-dimensional media are unstable [1–5]. The metaphor of a “snake” instability (SI) has been introduced in this context by Zakharov [1] in order to refer to the antisymmetric modulation (bending) of the solitonic wave-front caused by long-wavelength perturbations [3]. Later it has been predicted by numerical studies of the time evolution that the SI eventually leads to the formation of arrays of vortices with alternating charge [2,4]. The first experimental evidence of the SI and subsequent formation of vortices was observed in non-linear optics [6,7].

More recently, dark solitons have been observed in trapped dilute-gas BECs [8] and the decay of a stationary soliton into closed loops of vortex filaments, much resembling smoke rings, has been observed in a spherical harmonic trap [9]. Stationary dark solitons, like the example shown in Fig. 1(a), are nodes (nodal lines or planes in 2D or 3D, respectively) in the wavefunction as opposed to traveling solitons, which are also referred to as gray solitons. Theoretically, the stability of stationary solitons in harmonically trapped BECs had been investigated before by Muryshev *et al.* [10] and Feder *et al.* [11], based on a linear stability analysis using the Bogoliubov–de Gennes (BdG) equations. While both papers identify a regime of stability for stationary solitons in elongated traps at low density as expected from earlier work [3], it was conjectured in Ref. [10] that the mechanism of instability at increasing density was vortex pair production in analogy to the SI. Feder *et al.* [11] refined and partially

corrected the results of Ref. [10] and predicted the later experimentally observed vortex ring formation [9]. The mechanism of decay at the onset of instability, however, has not been fully revealed so far.

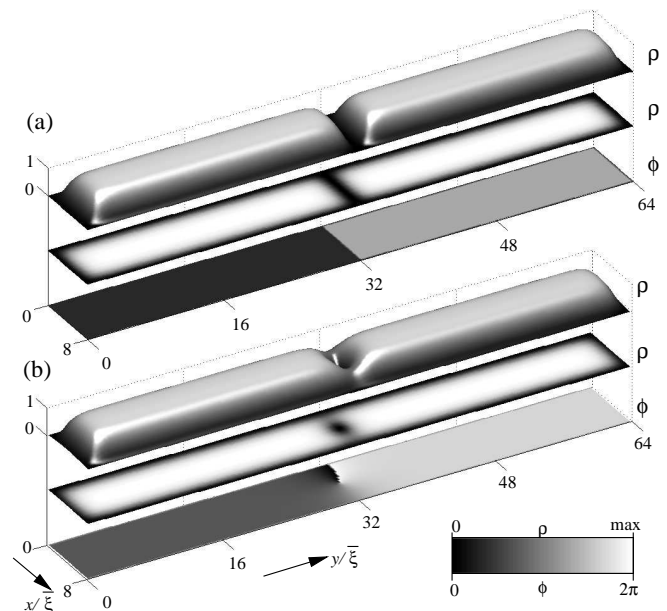


FIG. 1. Two stationary “one-defect” excited states in a 2D rectangular box trap with hard-wall boundary conditions generated by imaginary-time propagation of the NLSE: (a) stationary soliton (line node) and (b) stationary svortex state. The complex wavefunction ψ is represented by the density $\rho = |\psi|^2$ and the phase $\phi = \arg(\psi)$. Each subplot shows a surface plot and gray-scale coded plots of the density and the phase modulo 2π .

In this letter we study the modes of instability of a stationary soliton as a function of the transverse confinement L_t , measured in terms of the condensate healing

length ξ [12,13]. The onset of instability at $L_t \gtrsim 6\xi$ is initiated by the emergence of a nontrivial stationary state [see Fig. 1(b)] of *lower* energy than the corresponding stationary soliton. We call this state a solitonic vortex or “svortex”. A svortex is a single confined and deformed vortex with solitonic properties [13]. For transverse confinements of $6\xi \lesssim L_t \lesssim 10\xi$ the strong coupling of the stationary soliton to the more stable single svortex is the only decay mechanism available in contrast to what has been seen and expected in earlier work [3,10,11,9]. The svortex therefore presents the smallest possible unit of decay, which persists in geometries where the transverse confinement is too tight for vortex ring (in 2D: vortex pair) formation. Under less restrictive confinement, 2 and then 3 vortex channels open (for $L_t \gtrsim 10\xi$ and $L_t \gtrsim 13\xi$, respectively). The 1, 2, and 3 vortex instabilities will be seen to correlate perfectly with a BdG stability analysis.

The essential physics involved reveals itself from studying the time-dependent Gross-Pitaevskii or nonlinear Schrödinger equation (NLSE), which presents the relevant mean-field theory for a zero-temperature BEC [14] and also applies to non-linear wave propagation in optics [15]:

$$i\partial_t\psi = [-\nabla^2 + V + gv_B|\psi|^2]\psi. \quad (1)$$

In the dimensionless Eq. (1), the condensate wavefunction $\psi(\mathbf{r}, t)$ satisfies the following normalization condition: $\int_{v_B} |\psi|^2 d\mathbf{r} = 1$, where v_B is the volume of a box containing the trapped condensate. The external trapping potential is given by V and g is the nonlinear coupling constant. We restrict ourselves to a repulsive nonlinearity (or defocusing NLSE) $g > 0$. The relevant size scale for nonlinear structures like solitons [15] and vortices [16] is the condensate healing length $\xi = 1/\sqrt{gv_B|\psi|^2}$, where $\tilde{\xi} = 8\pi aN/(gv_B)$ is unit of length used in Eq. (1) for a BEC with N particles and an s -wave scattering length a . Note that for fairly uniformly distributed condensates, the healing length is given by $\bar{\xi} = 1/\sqrt{g}$. The application of NLSE solutions of type of Fig. 1 has been fully confirmed empirically by the experiments of Refs. [8,9]. In tightly confined BECs, the current mean-field theory is justified as long as the transverse dimensions are greater than ξ and $\xi \gg a$ is satisfied (see [17]).

We initially consider a 2D rectangular geometry with box boundary conditions. The chosen aspect ratio length/width of 8 simulates a transversely confined, waveguide-like geometry. The stationary vortex-like state with a node and phase singularity at the trap center was found by imaginary-time propagation and confirmed by real-time propagation of the NLSE [13]. In addition to seeding this relaxation procedure with a suitable phase profile, we also restricted the symmetry of the density $|\psi|^2$ to be even in both spacial directions. A second stationary state (a dark band soliton) was also generated by imaginary-time propagation with the constraint of odd symmetry in the longitudinal direction of the trap. Figure 1 shows the resulting wavefunctions. The vortex-like

wavefunction of Fig. 1(b) is clearly distorted and affected by the tight traverse confinement of $8\bar{\xi}$. We have argued in Ref. [13] that such a tightly confined vortex acquires solitonic properties and therefore should be called solitonic vortex or svortex, further discussed in [18].

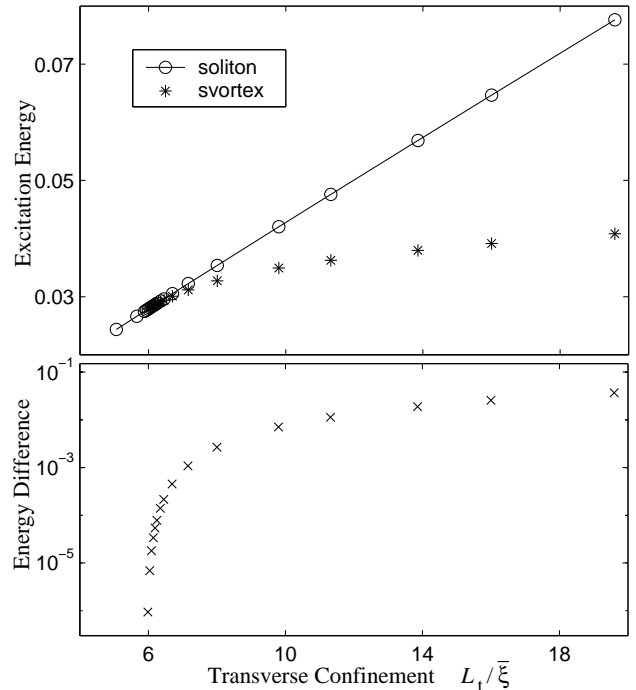


FIG. 2. Svortex and soliton properties as a function of the transverse confinement L_t . Part (a) shows the excitation energies of the stationary soliton and svortex state. The energy difference is shown on a logarithmic scale in part (b). The simulations were done in a rectangular box of size $8\bar{\xi} \times 64\bar{\xi}$ for different values of the nonlinear coupling constant g , which changes the effective transverse confinement $L_t/\bar{\xi} = 8\sqrt{g}$.

Figure 2(a) shows the excitation energy of the stationary svortex and soliton state with respect to the ground state as a function of the transverse confinement L_t in terms of $\bar{\xi}$. For a given wavefunction ψ , the energy is given by the formula $E = \int_{v_B} (-\psi^* \nabla^2 \psi + gv_B/2|\psi|^4 + V|\psi|^2) d\mathbf{r}$. The soliton excitation energy exhibits a linear dependence on the variation of the length scale reflecting the localization of the excitation in one and extension in the other spacial dimension. The svortex energy is always lower than the soliton energy and grows more slowly with the box size, reflecting the expected logarithmic behavior for large boxes [16]. Below a critical confinement corresponding to a box width of $\approx 6\bar{\xi}$ we do not find any stationary svortex solutions but instead the imaginary-time propagation converges to the soliton solution. The logarithmic plot of the energy difference between the soliton and the svortex energies shown in Fig. 2(b) very much indicates a nonanalytic curve joining or curve crossing. Following the svortex solution from wide confinement to

the critical point, the vortex wavefunction shows an increasingly deformed density and squeezed phase signature (see Fig. 1) and eventually coincides with the soliton wavefunction at the critical confinement.

The band solitons and svortex states from Fig. 2(a) are stationary states. In wide enough confinement, however, band solitons may exhibit the SI mentioned earlier: Tiny imperfections of stationary band solitons may lead to a transverse modulation and grow during real-time propagation at an initially exponential rate. The stability of stationary solutions of the NLSE can be tested in a linear stability analysis employing the famous BdG equations [19], which can be derived from a linear-response expansion of the time-dependent NLSE [20]. In the units of Eq. 1 the BdG equations read:

$$\mathcal{L}u_j(\mathbf{r}) - gv_B[\psi(\mathbf{r})]^2v_j(\mathbf{r}) = \epsilon_j u_j(\mathbf{r}), \quad (2)$$

$$\mathcal{L}v_j(\mathbf{r}) - gv_B[\psi^*(\mathbf{r})]^2u_j(\mathbf{r}) = -\epsilon_j v_j(\mathbf{r}), \quad (3)$$

with $\mathcal{L} = -\nabla^2 + V(\mathbf{r}) + 2gv_B|\psi(\mathbf{r})|^2 - \mu$, and μ is the chemical potential of the stationary wavefunction $\psi(\mathbf{r}, t) = \exp(-i\mu t)\psi(\mathbf{r})$. The solutions of the BdG equation with eigenvalues ϵ_j and eigenvectors (u_j, v_j) have the following interpretation in terms of small-amplitude motion around a stationary solution of the NLSE [16]: Small positive ϵ_j at positive “norm” $\eta_j = \int (|u_j|^2 - |v_j|^2) d\mathbf{r}$ describe small oscillations around the stationary state with increasing energy. Solutions with negative eigenvalue ϵ_j and positive η_j are called anomalous modes. They indicate a continuous transformation of the stationary state to a state of lower energy. Anomalous modes exist for the trapped vortex as well as for dark solitons in 1D and merely express the thermodynamic instability of these excitations. Complex or purely imaginary eigenvalues ϵ_j , however, indicate a dynamical instability. They further imply $\eta_j = 0$.

Figure 3 shows the purely imaginary and anomalous eigenvalues of the BdG equation for a stationary band soliton in a rectangular box of dimension $b \times 16\bar{\xi}$ as a function of the box width $b \approx L_t$ at constant density. For narrow traps with $b \lesssim 5.5\bar{\xi}$, we find one anomalous but no complex eigenvalues, like for 1D solitons. Additionally, the soliton wavefunction shows no appreciable decay in real-time propagation seeded with noise (see insets). Also collisions of noisy gray solitons show the robust, particle-like behavior expected from 1D soliton theory [18]. For trap widths $5.5\bar{\xi} \lesssim b \lesssim 9.5\bar{\xi}$ one purely imaginary eigenvalue exists in the BdG eigenvalue spectrum. According to the numerical results, the emergence of this imaginary eigenvalue coincides with the emergence of the svortex as a symmetry-breaking stationary state of lower energy than the corresponding band soliton. Increasing the box width, a second and eventually a third imaginary eigenvalue appears. The stability of the stationary soliton was probed using real-time propagation seeded with a small amount of white noise [21]. While there is no appreciable decay in tight confinement, we clearly find that the soliton instability is associated with the forma-

tion of one, two, and three vortices in the regimes where one, two, and three imaginary eigenvalues are present as shown in the insets of Fig. 3. The BdG eigenvectors u_j , localized within about one healing length from the nodal line of the soliton, also support this result [18]. The patterns shown in Fig. 3 are by no means stationary but rather form transient states followed by incomplete recurrences of the nodal line and eventual further decay where vortices move to edge of the trap and vorticity is destroyed. The complicated dynamical patterns showing a mixture of decay and strong mode coupling are certainly due to energy conservation in the NLSE and to the small scale of the trap used in the simulation where radiated phonons linger. We expect further stabilization of the vortex patterns in longer traps where energy released in the decay process can distribute itself over a larger area. The observed decay patterns vary depending on the exact form of the initial perturbation by noise. In contrast to the soliton, the stationary svortex shows an entirely real BdG spectrum with one anomalous mode also shown in Fig. 3. Further, real-time propagation of perturbed svortices shows no appreciable decay. In this sense, the svortex is the more stable object than the stationary soliton.

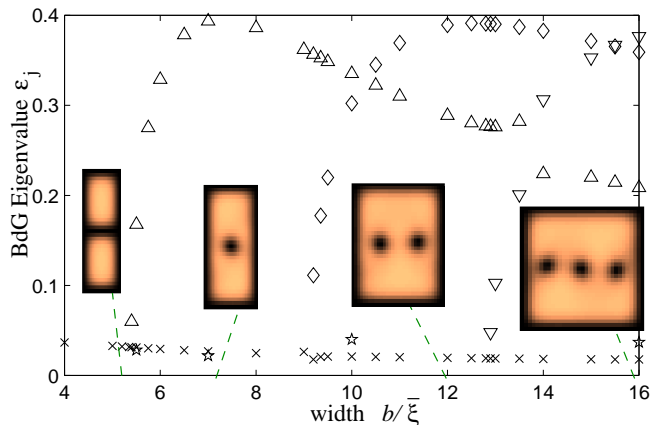


FIG. 3. Eigenvalues in the BdG spectrum of the stationary soliton in a 2D box as a function of the box width at constant average density. The insets relating to box widths of $b = 7\bar{\xi}$, $12\bar{\xi}$, and $16\bar{\xi}$ show density plots of transient patterns in the decay of the perturbed soliton state [21] after real-time propagation for $t = 26$, 31 , and 26 in the units of Eq. 1, respectively. The perturbed soliton at $b = 5\bar{\xi}$, on the contrary, shows no appreciable decay after 100 time units. The imaginary modes are marked according to the nature of the eigenvector u leading to single-vortex (Δ), double-vortex (\diamond) or triple-vortex (∇) decay. The anomalous mode of the nodal plane-state (\times) and stationary single-svortex state (\star) are also indicated.

Finally, we would like to comment on the 3D harmonic trap geometry studied earlier in the JILA experiment [9] and in theoretical work by Muryshev *et al.* [10] and Feder *et al.* [11]. Both experiment [9] and theory [11] report

vortex-ring formation during the decay of a stationary soliton (nodal-plane state) in spherical [9,11] and elongated [11] geometries at fairly high densities, which is indicated by the nature of complex modes in the BdG spectrum of the stationary soliton [11]. It has also been pointed out that the BdG spectrum becomes entirely real at sufficiently low particle number or high aspect ratio in elongated traps. However, the decay mechanism in the presence of a single imaginary mode in the BdG spectrum (as shown in Fig. 4 of Ref. [11]) of a stationary soliton in an elongated trap has not been revealed so far. Imaginary- and real-time propagation clearly show that a stationary svortex solution exists in this regime and that it has lower energy than the stationary soliton. The density and phase profile of the stationary svortex state are very similar to the dynamically generated pattern shown in Fig. 4. This figure shows the transient decay product of a perturbed stationary black soliton after real-time propagation for 100 ms, seeded initially with 0.01% white noise. The parameters of this 3D harmonic trap ($N = 10^4$ atoms of Na) correspond to Fig. 4 of Ref. [11] at an aspect ratio of $\omega_\rho/\omega_x = 4$ with $\omega_x = 2\pi \cdot 50\text{rad/s}$. The corresponding imaginary Bogoliubov mode u_j has an azimuthal coordinate dependence of $\exp(i\phi)$, where ϕ is the azimuthal angle, and much resembles the first imaginary BdG mode in the 2D box discussed above. The predicted decay of the band soliton into a single svortex has not been seen, or predicted, before and should be easily observable with current experimental techniques.

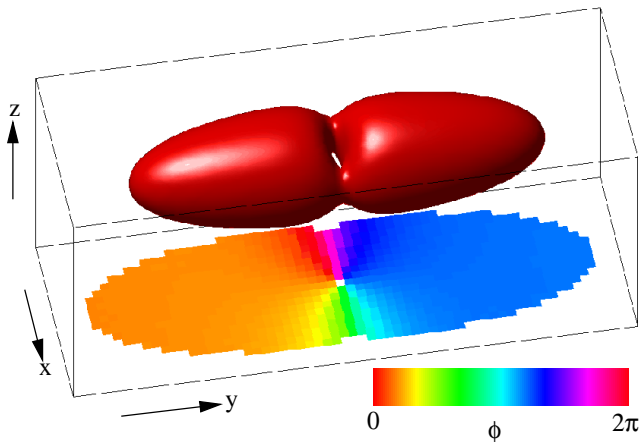


FIG. 4(color). Svortex in a 3D elongated harmonic trap generated by decay of a perturbed stationary soliton state. Shown is the surface of constant density (at 0.16 of the maximum density) and a color-coded plot of the phase in the horizontal plane intersecting the trap center. The transverse confinement $L_t/\xi \approx 7.7$ was computed by the maximum value of the line integral $\int_C \xi(\mathbf{r})^{-1} ds$ taken along the transverse dimension, which is more appropriate for measuring the transverse confinement of inhomogeneous condensates than the box width [13]. For details of the simulation see text.

Concluding, we have identified the fundamental modes

of the SI for transversely confined geometries: Production of 1, 2, and 3 vortices correlates with imaginary modes in the BdG eigenvalue spectrum. Departure from the quasi-1D regime of stability of solitons is indicated not only by a linear stability analysis but also by the emergence of a solitonic vortex or svortex as a stationary state of lower energy than the corresponding dark soliton. We demonstrated that the decay of a soliton into a single svortex is a fundamental mode of instability in 2D box geometry and 3D elongated harmonic traps.

We like to thank Yuri Kivshar for one discussion and David Feder for helpful discussions and the access to unpublished results. Support from the National Science Foundation and the Alexander von Humboldt Foundation within the Feodor Lynen program (J. B.) is gratefully acknowledged.

-
- [1] V. E. Zakharov and A. M. Rubenchik, Zh. Eksp. Teor. Fiz. **65**, 997 (1973), [Sov. Phys. JETP **38**, 494 (1974)].
 - [2] C. A. Jones, S. J. Putterman, and P. H. Roberts, J. Phys. A: Math. Gen. **19**, 2991 (1986).
 - [3] E. A. Kuznetsov and S. K. Turitsyn, Zh. Eksp. Teor. Fiz. **94**, 119 (1988), [Sov. Phys. JETP **67**, 1583 (1988)].
 - [4] C. T. Law and G. A. Swartzlander, Jr, Opt. Lett. **18**, 586 (1993).
 - [5] Y. S. Kivshar and D. E. Pelinovsky, Phys. Rep. **331**, 117 (2000).
 - [6] A. V. Mamaev, M. Saffman, and A. A. Zozulya, Phys. Rev. Lett. **76**, 2262 (1996), and A. V. Mamaev *et al.*, Phys. Rev. A **54**, 870 (1996).
 - [7] V. Tikhonenko, J. Christou, B. Luther-Davies, and Y. S. Kivshar, Opt. Lett. **21**, 1129 (1996).
 - [8] J. Denschlag *et al.*, Science **287**, 97 (2000), and S. Burger *et al.*, Phys. Rev. Lett. **83**, 5198 (1999).
 - [9] B. P. Anderson *et al.*, Phys. Rev. Lett. **86**, 2926 (2001).
 - [10] A. E. Muryshev, H. B. van Linden van den Heuvell, and G. V. Shlyapnikov, Phys. Rev. A **60**, R2665 (1999).
 - [11] D. L. Feder *et al.*, Phys. Rev. A **62**, 053606 (2000).
 - [12] W. P. Reinhardt and C. W. Clark, J. Phys. B **30**, L785 (1997).
 - [13] J. Brand and W. P. Reinhardt, J. Phys. B **34**, L113 (2001).
 - [14] F. Dalfovo, S. Giorgini, L. P. Pitaevskii, and S. Stringari, Rev. Mod. Phys. **71**, 463 (1999).
 - [15] Y. S. Kivshar and B. Luther-Davies, Physics Reports **298**, 81 (1998).
 - [16] A. L. Fetter and A. A. Svidzinsky, Journal of Physics: Condensed Matter **13**, R135 (2001).
 - [17] D. S. Petrov, G. V. Shlyapnikov, and J. T. M. Walraven, Phys. Rev. Lett. **85**, 3745 (2000).
 - [18] J. Brand and W. P. Reinhardt, to be published.
 - [19] N. Bogolubov, J. Phys. **11**, 23 (1947).
 - [20] M. Edwards *et al.*, Phys. Rev. Lett. **77**, 1671 (1996).
 - [21] We seeded the initial wavefunction with 0.01% white noise with respect to the largest Fourier component of the wavefunction ψ . See also L. D. Carr, J. N. Kutz, and W. P. Reinhardt, Phys. Rev. E **63**, 066604 (2001).